J Solid State Electrochem (2012) 16:1019–1032
DOI 10.1007/s10008-011-1477-6

ORIGINAL PAPER

Numerical investigations of solution resistance effects on nonlinear electrochemical impedance spectra

Sruthi Santhanam · Vimala Ramani · Ramanathan Srinivasan

Received: 1 May 2011 / Revised: 13 June 2011 / Accepted: 15 June 2011 / Published online: 29 June 2011

Abstract The effect of solution resistance on the nonlinear electrochemical impedance spectra under quasi-potentiostatic conditions was investigated by numerical simulations. An electron transfer reaction, a reaction with an adsorbed intermediate and a reaction exhibiting negative resistance were chosen as the candidates and large amplitude perturbations were employed. The potential across the interface drifts initially and stabilizes after a certain time, which depends on the solution resistance and the kinetic parameter values. The fraction of the applied potential drop occurring across the metal–solution interface depends on the frequency and the amplitude of the perturbation as well as the value of solution resistance. This in turn leads to the possibility that, for a given conditions, a part of the spectrum may be acquired in the linear regime while the remaining part may be acquired in the nonlinear regime. The sensitivity of the Kramers Kronig transform (KKT) to identify these cases is evaluated. The results show that although the spectra are distorted by poorly conducting solution, the sensitivity of KKT to identify the nonlinear effects is not enhanced by the introduction of significant solution resistance.

Keywords EIS · Anodic dissolution · Solution resistance · Nonlinear · KKT

Introduction

Electrochemical impedance spectroscopy (EIS) is often applied to characterize corrosion, fuel cells, batteries, coatings, sensors, etc. [1–4]. In EIS, a sinusoidal perturbation, usually of small amplitude, is applied and the response of the system is analyzed. The system may be held at a constant potential and a potential perturbation may be superimposed on it (quasi-potentiostatic mode) [5–8] or it may be held at a constant current with a current perturbation superimposed on it (quasi-galvanostatic mode) [9]. The response of the system at various frequencies is recorded and analyzed. The analyses of the spectra reported in the literature invariably assume that the system is linear, causal and stable. However, in actual experiments, these assumptions may not always hold true. The response of a system satisfying these assumptions can be validated by Kramers Kronig transforms (KKT). Electrochemical systems are inherently nonlinear, but by minimizing the amplitude of input perturbation it is hoped that the system under study can be approximated by a linear system. On one hand, too small a perturbation will lead to a poor signal-to-noise ratio. On the other hand, too large a perturbation will cause the nonlinear effect to impact the measured spectrum and hence in those cases, the analysis must include the nonlinear effects.

Typical perturbation amplitudes employed in the EIS measurements are in the range of 5–20 mV so that a

Electronic supplementary material The online version of this article (doi:10.1007/s10008-011-1477-6) contains supplementary material, which is available to authorized users.

S. Santhanam
Department of Chemical Engineering,
Sri Venkateswara College of Engineering, Anna University,
Chennai 602105, India

V. Ramani
Department of Mathematics, Anna University,
Chennai 600025, India

R. Srinivasan (✉)
Department of Chemical Engineering,
Indian Institute of Technology-Madras,
Chennai 600036, India
e-mail: srinivar@iitm.ac.in

compromise between obtaining a high signal to noise ratio and maintaining linearity of the system response could be achieved. There are a limited number of reports on the experimental studies with large amplitude perturbations [10–14]. Some of the advantages of large amplitude perturbations include better signal to noise ratio, the ability to obtain information on the system nonlinearity efficiently and the ability to isolate the nonlinearity better [12]. For example, nonlinearities can arise due to exponential relationship between the current and overpotential and also due to nonlinear coupling between kinetics to mass transfer [12]. It may not be possible to isolate these effects by steady state or small amplitude EIS. Large amplitude EIS performed over sufficiently large frequency range may enable the separation and characterization of these two effects. To illustrate the nonlinear effects occurring in electrochemical systems and to study the sensitivity of KKT to identify the nonlinearities, the dissolution of Fe in 1 M H_2SO_4 was studied with voltage perturbation amplitudes of 150 mV and less [10]. The corrosion of carbon steel in a solution containing Na_2SO4 and H_2SO_4 was studied using potential perturbations with amplitudes up to 330 mV [11]. Solid oxide fuel cells were characterized using large amplitude current perturbations (pseudo galvanostatic mode) where the potential response, in some cases, corresponds to 450 mV amplitude [12]. In another pseudo galvanostatic study of fuel cells, current perturbation amplitudes of 1 to 2.5 A were employed and at some frequencies, the corresponding potential amplitude was about 150 mV [13]. It is relatively straightforward to employ large amplitude perturbations in experimental studies. However, including the nonlinear terms in the analysis is difficult and hence most studies are limited to small amplitude EIS.

The nonlinear effects can be incorporated in the analysis by (a) expanding the rate in Taylor series and including the higher order terms [11, 14–17] or (b) expanding the rate in Fourier series [18] or (c) complete numerical simulation of the governing equations [19–21]. For the case of an electrochemical reaction via an adsorbed intermediate, with negligible solution resistance, the impedance spectrum for large amplitude perturbations has been simulated by numerical methods [21]. In the case of an electron transfer reaction, the analytical solution for the case without solution resistance [18] and the numerical solution for the case with significant solution resistance [19, 20] have also been reported. If the conductivity of the electrolyte is low, a supporting electrolyte can be added. But the unsupported case is also of interest, and many a times the solution resistance is comparable to the charge transfer resistance. For an unsupported system, the impedance response to small amplitude perturbations, accounting for kinetic effects, adsorption effects and diffusion effects have been investigated [22, 23]. In this work, the effect of solution resistance on the large amplitude EIS response of metal corrosion process is investigated by numerical simulation. A simple electron transfer reaction, a reaction with an adsorbed intermediate species and a reaction exhibiting negative resistance are chosen as the candidate mechanisms.

Theory

We consider the electrochemical dissolution of a metal where it is assumed that the kinetic parameters depend exponentially on the potential and that the Langmuir isotherm model is applicable. The Langmuir isotherm assumption is employed for its simplicity and does not limit the validity of the conclusions drawn here. The electrochemical system can be modeled by the circuit shown in Fig. 1, where Z_f represents the Faradaic impedance, C_{dl} denotes the double layer capacitance and R_{sol} is the solution resistance. The potential drop across the solution resistance is V_1, and that across the electrode–electrolyte interface is V_2. The current through the double layer capacitance is i_{2a}, that through the Faradaic process is i_{2b}, while that through the solution is i_1. Before the perturbation is applied, only a dc potential (V_{dc}) is applied onto the system, and a part of the potential drop (V_{1dc}) will occur across the solution. The remaining part (V_{2dc}) will occur across the electrode–solution interface. An ideal capacitance will not allow dc current to pass through it, and hence the double layer capacitance value will not impact the value of the dc current. Here, the open circuit potential is taken as the reference (zero). The development of the basic mass balance and charge balance equations and the linearization results are reported in the literature [24–28]. The development of equations accounting for the solution resistance and nonlinear effects is given in the following sections.

Electron transfer reaction

Consider the electron transfer reaction

$$M \xrightarrow{k_1} M^+_{sol} + e^-, \tag{1}$$

where M is the bare metal site, M^+_{sol} is the dissolved metal ion and k_1 is the reaction rate constant, which depends on

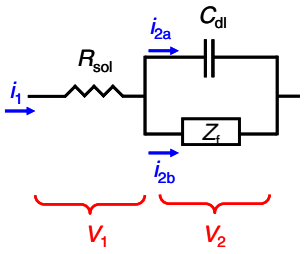

Fig. 1 Electrical circuit model of the electrochemical reaction system

the potential V_2 as $k_i = k_{i0}e^{b_i V_2}$. The exponent b_i is given by the formula $b_i = \frac{\alpha_i F}{RT}$, where α_i is the transfer coefficient, F is the Faraday constant, R is the universal gas constant and T is the temperature.

The current due to Faradaic reaction is

$$i_{2b} = Fk_1 \tag{2}$$

When an ac potential is superimposed on the dc potential, the current balance is given by

$$C_{dl}\frac{dV_{2ac}}{dt} + Fk_{10}e^{b_1(V_{2dc}+V_{2ac})} = \frac{V - V_2}{R_{sol}} = \frac{V_{dc} - V_{2dc}}{R_{sol}} + \frac{V_{ac0}\sin(\omega t) - V_{2ac}}{R_{sol}}, \tag{3}$$

where V_{ac0} and $\omega(=2\pi f)$ are the amplitude and the angular frequency, respectively, of the applied perturbation, t is the time and V_{2ac} is the time varying component of the potential drop across the interface. Equation 3 is a first-order nonlinear ordinary differential equation in $V_{2ac.}$ When only the dc potential is applied, the derivative in Eq. 3 vanishes, and the algebraic equation can be numerically solved to determine the dc potential drop across the interface (V_{2dc}). When the ac perturbation is also present, the nonlinear differential Eq. 3 could not be solved analytically. However, if the nonlinear terms of the current in the Faradaic process are neglected, the solution of Eq. 3 is

$$V_{2ac} = \frac{V_{ac0}}{R_{sol}C_{dl}}\left[\frac{P\sin(\omega t) - \omega\cos(\omega t)}{P^2 + \omega^2}\right] + \frac{V_{ac0}}{R_{sol}C_{dl}}\left[\frac{\omega}{P^2 + \omega^2}\right]e^{-Pt}, \tag{4}$$

where

$$P = \frac{1}{C_{dl}}\left[Fb_1k_{1dc} + \frac{1}{R_{sol}}\right] \text{and } k_{1dc} = k_{10}e^{b_1V_{2dc}} \tag{5}$$

The charge transfer resistance is given by

$$R_t = (Fb_1k_{1dc})^{-1} \tag{6}$$

Note that R_t is part of the parameter P in Eq. 5. Equation 4 shows that the average value of V_{2ac} will change exponentially with time and will stabilize after some time. For a given R_{sol}, the numerical simulations were conducted until the V_{2ac} stabilized and by utilizing the subsequent cycles, the current values were calculated using Eq. 2. The current is then subjected to finite Fourier transform (FFT) to obtain the magnitude and phase at the fundamental harmonic, from which the impedance is calculated.

In general, the current response of an electrochemical system to the potential perturbation can be described by a transfer function. In EIS studies, the most commonly employed transfer function is the ratio of the vector voltage to the vector current [10, 29]. If the system is linear, causal and stable, the transfer function is called "impedance," and when one or more of these conditions are violated, the term "impedance" is not applicable sensu stricto. However, both the terms "impedance" and "nonlinear impedance" have been employed in literature even for the cases where nonlinear effects are significant [11, 12, 14–19]. For many of the results presented here, the system response is linear and the transfer function corresponds to the impedance. Since the results of linear and nonlinear responses are presented together, the term "impedance" is used to indicate all of them including the transfer functions of nonlinear systems. Likewise, the term "admittance" is used to indicate the transfer function which is the ratio of vector current to vector voltage.

Reaction with single adsorbed intermediate

In the second case, the following reaction with an adsorbed intermediate is analyzed.

$$\begin{aligned} M &\xrightarrow{k_1} M^+_{ads} + e^- \\ M^+_{ads} &\xrightarrow{k_2} M^+_{sol} \end{aligned} \tag{7}$$

Here, M^+_{ads} is the adsorbed intermediate whose fractional surface coverage is denoted by θ_1.

The current corresponding to this reaction is

$$i_{2b} = Fk_1(1 - \theta_1) \tag{8}$$

The mass balance equation is

$$\tau\frac{d\theta_1}{dt} = k_1\theta_V - k_2\theta_1, \tag{9}$$

where $\theta_V = (1 - \theta_1)$ is the fractional surface coverage of bare metal sites and τ is the total number of sites. In the absence of an ac perturbation, the steady state surface coverage of M^+_{ads} is

$$\theta_1^{SS} = \frac{k_{1DC}}{k_{1DC} + k_{2DC}} = \frac{\left(\frac{1}{k_{2DC}}\right)}{\sum_{i=1}^{2}\left(\frac{1}{k_{iDC}}\right)} \tag{10}$$

Here k_{iDC} refers to the rate constant at the dc over-potential across the metal solution interface. When the solution resistance is zero, it is given by $k_{iDC} = k_{i0}e^{b_iV_{dc}}$, and in presence of solution resistance it is given by $k_{iDC} = k_{i0}e^{b_iV_{2dc}}$.

The dc Faradaic current is

$$i_{2b,dc} = Fk_{1dc}\left(1-\theta_1^{SS}\right) = \frac{1}{\sum_{i=1}^{2}\left(\frac{1}{k_{iDC}}\right)} = \frac{k_{1dc}k_{2dc}}{k_{1dc}+k_{2dc}} \tag{11}$$

Under steady-state conditions, the potential drop across the interface V_{2dc} can be found by numerically solving the nonlinear algebraic equation

$$\frac{V_{dc}-V_{2dc}}{R_{sol}} = F\frac{k_{10}k_{20}e^{(b_1+b_2)V_{2dc}}}{k_{10}e^{b_1V_{2dc}}+k_{20}e^{b_2V_{2dc}}} \tag{12}$$

When an ac potential V_{ac} is superimposed on V_{dc} and applied onto the system, the current balance leads to the following differential equation for V_{2ac}.

$$C_{dl}\frac{dV_{2ac}}{dt}+\left[Fk_{10}e^{b_1(V_{2dc}+V_{2ac})}(1-\theta_1)\right] = \frac{V_{dc}-V_{2dc}}{R_{sol}}+\frac{V_{ac0}\sin(\omega t)-V_{2ac}}{R_{sol}} \tag{13}$$

By solving Eqs. 9 and 13 simultaneously, V_{2ac} and θ_1 are obtained. By substituting these values in Eq. 8, the current value i_{ac} is obtained as a function of t.

Even when the solution resistance is zero, the application of a sinusoidal perturbation to the nonlinear system will cause a drift of the average values of the surface coverage and the current (Niket Kaisare, Vimala Ramani, Ramanathan Srinivasan, manuscript under review, *Electrochimica Acta*). When there is significant solution resistance, the average of V_{2ac} will also drift, as seen for the electron transfer reaction. For high-frequency perturbations of small V_{ac0} values, the value of V_{2ac} obtained by neglecting $\frac{d\theta_1}{dt}$ and solving Eq. 13 is

$$V_{2ac}=\frac{V_{ac0}}{R_{sol}C_{dl}}\left[\frac{P\sin(\omega t)-\omega\cos(\omega t)}{P^2+\omega^2}\right]+\frac{V_{ac0}}{R_{sol}C_{dl}}\left[\frac{\omega}{P^2+\omega^2}\right]e^{-Pt}, \tag{14}$$

where

$$P = \frac{1}{C_{dl}}\left[Fb_1k_{1dc}(1-\theta_{1.av})+\frac{1}{R_{sol}}\right] \tag{15}$$

Thus, the average value of V_{2ac} drifts with time but eventually settles down to a value depending on the values of the parameters as given in Eq. 15. The surface coverage value also drifts, and we can estimate the time it takes to stabilize the surface coverage values as follows. If a potential step is applied to the system, the new surface coverage value is given by

$$\theta_{new} = \theta_{new}^{SS}+\left(\theta_{old}^{SS}-\theta_{new}^{SS}\right)e^{-\frac{k_{1-new}+k_{2-new}}{\tau}} \tag{16}$$

where the subscripts "old" and "new" represent respectively the values before and after the application of the potential step. The superscript SS refers to the steady state values. From Eq. 16, it is clear that the time constant for the surface coverage drift is $\frac{k_{1-new}+k_{2-new}}{\tau}$. The impedance is calculated by using the current values after stabilization of both the surface coverage and the current values.

Reaction with two adsorbed intermediates

Consider the reaction

$$\begin{aligned}
&M \underset{k_{-1}}{\overset{k_1}{\rightleftharpoons}} M_{ads}^{+}+e^-\\
&M_{ads}^{+} \underset{k_{-2}}{\overset{k_2}{\rightleftharpoons}} M_{ads}^{2+}+e^-\\
&M_{ads}^{2+} \xrightarrow{k_3} M_{sol}^{2+}\\
&M+M_{ads}^{2+} \xrightarrow{k_4} M_{ads}^{2+}+M_{sol}^{2+}+2e^-
\end{aligned} \tag{17}$$

The reaction is chosen to illustrate the application of the methodology to a fairly complex mechanism. The last step in Eq. 17 is also known as catalytic step, because one of the species involved in the step $\left(M_{ads}^{2+}\right)$ is regenerated. The Faradaic current for this case is given by

$$i_{2b} = F\{(k_1\theta_V-k_{-1}\theta_1)+(k_2\theta_1-k_{-2}\theta_2)+(k_4\theta_2\theta_V)\} \tag{18}$$

while the mass balance is given by

$$\begin{aligned}
\tau\frac{d\theta_1}{dt} &= (k_1\theta_V-k_{-1}\theta_1)-(k_2\theta_1-k_{-2}\theta_2)\\
\tau\frac{d\theta_2}{dt} &= (k_2\theta_1-k_{-2}\theta_2)-(k_3\theta_2)
\end{aligned} \tag{19}$$

where θ_1, θ_2 and θ_v are the fractional surface coverage values of M_{ads}^{+}, M_{ads}^{2+} and bare metal site (M), respectively, with the constraint that $\theta_1+\theta_2+\theta_v=1$. Note that the presence of a bare metal site (M) is necessary for the last step in Eq. 17 to proceed. The equation for the ac potential across the interface (V_{2ac}) is given by,

$$C_{dl}\frac{dV_{2ac}}{dt}+[F\{(k_1\theta_V-k_{-1}\theta_1)+(k_2\theta_1-k_{-2}\theta_2)+(k_4\theta_2\theta_V)\}] = \frac{V_{dc}-V_{2dc}}{R_{sol}}+\frac{V_{ac0}\sin(\omega t)-V_{2ac}}{R_{sol}} \tag{20}$$

The procedure employed for calculating the impedance is similar to that described in the previous section.

For all simulations, the frequency range employed is 100 kHz to 1 mHz, with 10 frequencies per decade spaced logarithmically. The V_{ac0} values employed were in the 5–200 mV range. The R_{sol} values ranged from 0.1 to 100Ω. While metal dissolution is employed as an example here, this methodology can be easily adopted for other reactions

involving any number of adsorbed intermediates. Similarly, the adsorption isotherms other than Langmuir model can also be employed. The source code, written in Matlab® programming language, can be obtained by contacting the corresponding author.

Results and discussion

Electron transfer reaction

Potential drop across the interface

Figure 2 shows the potential across the electrode–solution interface (V_2) as a function of time for a few combinations of V_{ac0} and R_{sol}, and at 100 kHz perturbation frequency, for the electron transfer reaction. The values of V_2 averaged over one period are also presented as dotted lines. The value of V_{2ac} as predicted by Eq. 4 matches the numerical results exactly at high frequencies. Hence, the numerical and analytical results are not shown separately in Fig. 2. In Fig. 2a, when R_{sol} is small, the average value of V_2 drifts and settles quickly. In Fig. 2b, when R_{sol} is large, it takes much longer time to settle. Since the time scale is large compared to the period of the perturbation, in Fig. 2b, the transient values of V_2 only at the initial stages is given in the inset. Figure 2c and d shows the results for V_{ac0}= 200 mV. In Fig. 2, comparisons of panels (a) with (c), and (b) with (d) show that the time it takes to settle is independent of V_{ac0}. Again, in Fig. 2d the transient V_2 values are given in the inset while the average V_2 values are given in the main figure, because of the difference in the time scales involved. The value of the parameter P in Eq. 5 determines whether the final average value is reached quickly or slowly. For example, a larger value of R_{sol} or a large charge transfer resistance will lead to a small value of P and correspondingly, longer time for stabilization. For a small R_{sol} and a fast reaction, the average of V_2 would stabilize quickly. Usually, it is assumed that waiting for one cycle of perturbation is sufficient to reach the stable state. However, the results here show that the duration for stabilization depends on the solution resistance and the kinetic parameters and is independent of the frequency, at least for the linear case. In actual experiments, the wait time needed to avoid the drift can be estimated from the measured double layer capacitance, solution resistance and charge transfer resistance values. If a sufficient wait time is not employed, then the data would be acquired under unstable conditions, which essentially invalidates the EIS data.

The analytical and numerical results, when R_{sol}=100 Ω, V_{ac0}=200 mV and f=1 Hz, are presented in Fig. 3. The clear difference seen between the analytical and numerical results indicates that the nonlinear effects manifest at these conditions and that the analytical result, which is based on the linearized form of the Eq. 3, is not accurate. Thus, at large R_{sol}, large V_{ac0} and low frequencies, the nonlinear effects affect the V_2 values significantly. At smaller values

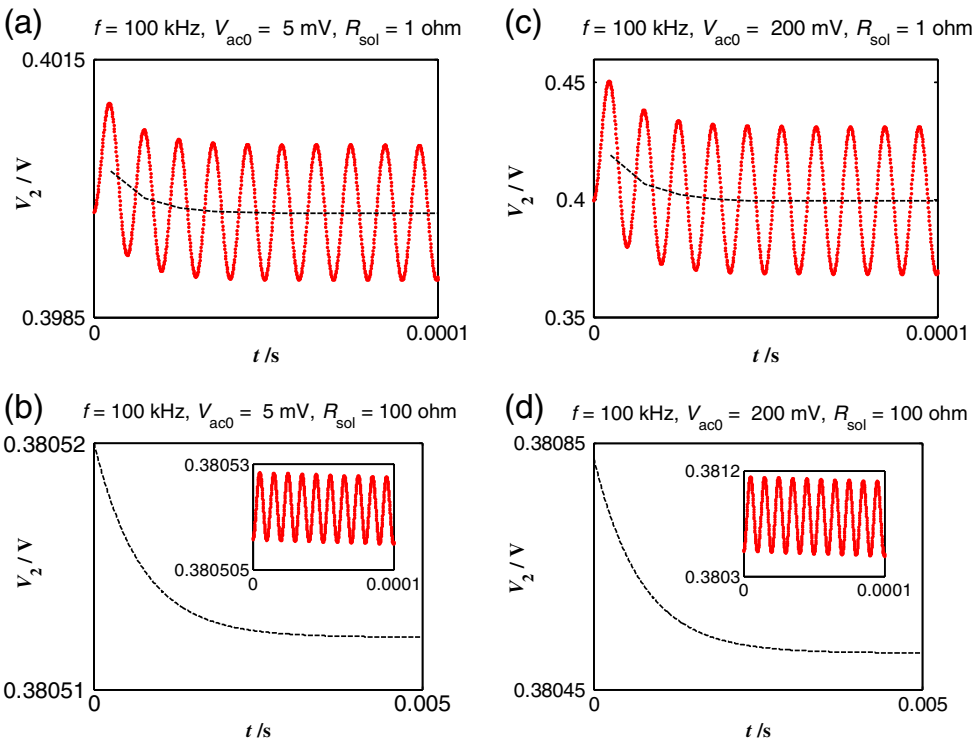

Fig. 2 Transient V_2 values as a function of time for f=100 kHz for two V_{ac0} values and two R_{sol} values for the mechanism in Eq. 1. The parameter values are $k_{10}=10^{-12}$ mol s^{-1}, b_1=20 V^{-1}, V_{dc}=0.4 V, $C_{dl}=10^{-5}$ F. The numerical and analytical results matched exactly and are not presented separately. *Dots* are the transient values and *dotted lines* are the average values. In (b) and (d), the transient V_2 values are shown in the *inset*

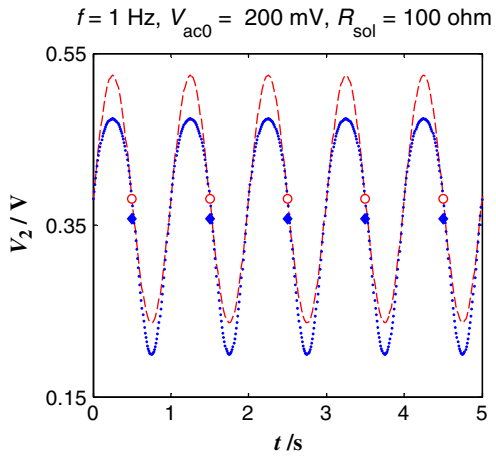

Fig. 3 Transient V_2 values as a function of time for f=1 Hz for the mechanism in Eq. 1. All other parameter values are the same as in Fig. 2. Transient V_2 values are depicted in *dotted lines* (numerical solution) and *dashed lines* (analytical solution). The V_2 values averaged over one period are given in symbols. *Filled diamonds* numerical solution, *open circles* analytical solution

of R_{sol} or smaller values of V_{ac0}, the analytical and numerical results match very well even at low frequency and hence are not presented. After the average of V_2 stabilized, the magnitude of the ac component of V_2 at the fundamental frequency $|V_{2ac}|_\omega$ is obtained using FFT and the normalized value $r = \frac{|V_{2ac}|_\omega}{V_{ac0}}$ was calculated. For V_{ac0}=10 mV, the trend of r vs f is plotted for various R_{sol} values in Fig. 4. The results for other values of V_{ac0} were similar (Fig. S1). A similar trend was reported in the literature for another electron transfer reaction [19, 20]. At high frequencies, the impedance of the double layer capacitance is very low. Hence, most of the potential drop would occur across the solution resistance and hence the value of r is low, particularly when R_{sol} is large. At low frequencies, the double layer capacitance would offer very high impedance. The Faradaic process would offer relatively less impedance and most of the current will pass through it. When R_{sol} is small, it is seen that most of the potential drop occurs across the interface in all the frequency ranges. When the R_{sol} is large, only a part of the applied potential drop will occur across the interface and the value of r is significantly less than 1 even at low frequencies, as seen in the case of R_{sol}=100Ω in Fig. 4.

Impedance spectra

Figure 5 shows the complex plane plots of impedance spectra for various R_{sol} values and V_{ac0} values. Note that the solution resistance is subtracted from the real part of the impedance so that a clear comparison can be made. It is shown in Fig. 5a that when R_{sol} is 10Ω or less, the spectra are more or less the same. At higher R_{sol}, the spectrum, especially at low frequencies, is different. This is understandable since the impedance is calculated assuming that all the potential drop occurs across the metal–solution interface, whereas in reality only a fraction of the potential drop occurs across the interface and the rest occurs across the solution. A comparison of Fig. 5a and b shows that the spectra are practically the same for both V_{ac0} values, for a given R_{sol}. Thus, in this example, the nonlinear effects are negligible when $V_{ac0} \leq 10$ mV. However, Fig. 5c and d shows that the spectra are different from those in Fig. 5a and b and that the nonlinear effects are dominant at $V_{ac0} \geq 100$ mV. It is also worth noting that the nonlinear effects are lesser at large values of R_{sol}. For example, when R_{sol} is 1Ω, an increase in V_{ac0} from 5 to 200 mV, results in a decrease in R_t from 175 to 42Ω, and the spectra in these two cases are clearly different as seen in Fig. 5a and d for R_{sol}=1Ω plots. On the other hand, when R_{sol} is 100Ω, a similar change in V_{ac0} from 5 to 200 mV results in a decrease of R_t from 257 to 226Ω, and the spectra in these two cases are only slightly different, as seen in Fig. 5a and d for R_{sol}=100Ω plots. When R_{sol} is large, the effective ac potential across the interface (V_{2ac}) is significantly less than the applied ac potential (V_{ac0}) and hence the nonlinear effects are relatively less.

One of the interesting facts is that large amplitude perturbations can lead to nonlinear effects which manifest in the EIS data, but KKT does not, in general, identify the deviations due to the nonlinear effects as reported in the numerical [20, 21] and experimental [10] investigations. In the presence of solution resistance, the following scenario may occur. For large amplitude perturbations, a part of the spectrum, acquired at high frequencies, may be in the linear regime because V_{2ac} would be significantly smaller than V_{ac0}, while the remaining part of the spectrum, acquired in the low frequencies, may be in the nonlinear regime since V_{2ac} will be more or less equal to V_{ac0} in those cases. The ability of KKT to identify this effect is evaluated

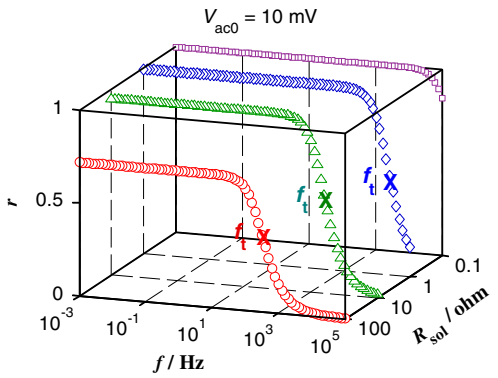

Fig. 4 The fraction of applied potential V_{ac0} that occurs across the interface (r) as a function of frequency at V_{ac0}=10 mV for different R_{sol} values for the mechanism in Eq. 1. All parameters employed are the same as those in Fig. 2 The transition frequency (f_t) values, calculated from Eq. 21 are also marked

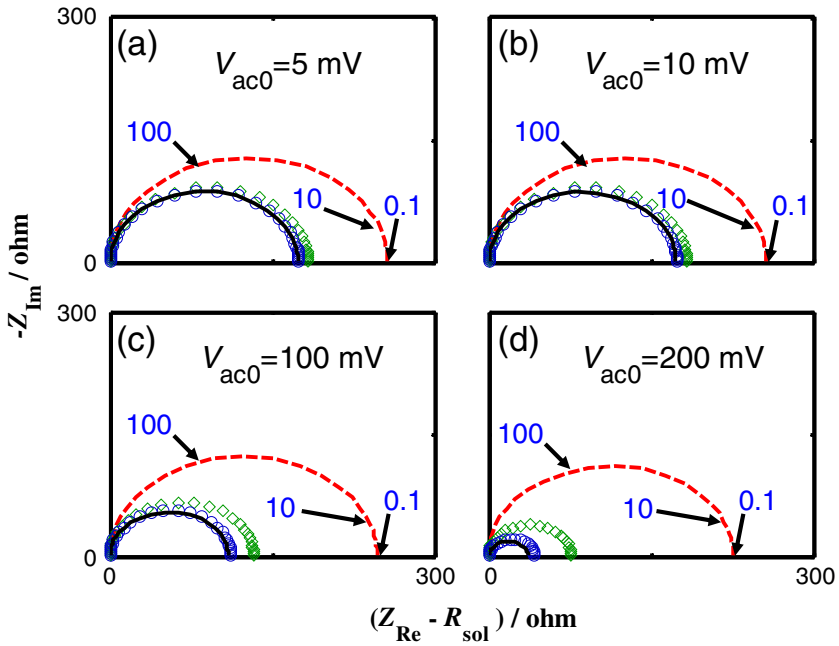

Fig. 5 Complex plane plots of the impedance spectra for the electron transfer reaction, in the presence of significant R_{sol}. Note that, in the abscissa, R_{sol} is subtracted from Z_{Re} to enable clear comparison between the spectra. R_{sol}: *solid line* 0.1Ω, *open circles* 1Ω, *open diamonds* 10Ω, *dashed line* 100Ω. The values for R_{sol}=0.1 and 1Ω completely overlap. A few frequencies, in Hz, are marked in the figures

Kramers Kronig transforms

The impedance spectra in Fig. 5 are subjected to KKT and the results are presented in Fig. 6. The dotted lines are the original values and the continuous lines are the transformed data. The original data and transformed data are practically indistinguishable for most of the plots, for all the V_{ac0} and R_{sol} values. Hence, the results for V_{ac0}=5 and 200 mV are presented in Fig. 6 while the results for V_{ac0}=10 and 100 mV are presented elsewhere (Fig. S2). Figure 6a and c shows that there is a slight deviation in the real component, at low frequencies. A vertical displacement in the real component computed from KKT, especially at low frequencies, can arise from an error in the polarization resistance [30]. The other possibility is that the numerical KKT integrations are performed on the data only from 10 mHz to 100 kHz while in theory, the integration must be carried out from a frequency of 0 to ∞ and this finite range employed may explain the discrepancy. The deviations are larger when V_{ac0}=5 mV and they are independent of R_{sol} values. Thus the deviations are certainly not an indicator of nonlinear effects. Even though the nonlinear effects are obvious at $V_{ac0}\geq$100 mV, and the spectra are different, KKT does not identify the violation of linearity criteria. It is likely that "the apparent polarization resistance changes by the same amount in both the real and imaginary components of the interfacial impedance" [10], and the impedance transforms correctly. In summary, based on the results shown in Fig. 6, it can be concluded that in this case, KKT does not identify the nonlinear effects particularly well and its sensitivity is independent of the solution resistance values.

A similar mechanism was analyzed in literature [20] and it was concluded that KKT can identify the nonlinear effects in presence of the solution resistance, under certain conditions. A formula for transition frequency (f_t), where the system response changes from a high-frequency linear behavior to low frequency nonlinear behavior, was also presented [20].

$$f_t = \frac{1}{2\pi C_{dl}}\left(\frac{1}{R_{sol}} + \frac{1}{R_t}\right) \tag{21}$$

Using Eq. 21, the f_t values are found to be about 159 kHz, 16 kHz, 1.7 kHz and 221 Hz for R_{sol} values of 0.1, 1, 10 and 100Ω, respectively. The transition frequencies fall in the frequency range we employed for all the cases except R_{sol}= 0.1Ω, as marked in Fig. 4. The transition frequencies are predicted well by Eq. 21. However, significant differences between the original and transformed impedance values are not seen in the spectra (Fig. 6). The methodology employed in the previous report [19] is mostly similar to our numerical simulations, with possibly the following key difference: when the perturbation was applied, it is not clear if a sufficient wait time was employed as in the present case. KKT is known to be sensitive to violations of stability conditions [10, 21, 31–33]. Besides, the deviations they reported were also in the 0.1% range, while gross deviations that are identifiable in common experiments (where the noise itself may be more than 0.1%) are sought in the present work. These differences may explain the difference in the conclusions regarding KKT compliance of EIS data in presence of significant R_{sol} and for large V_{ac0}.

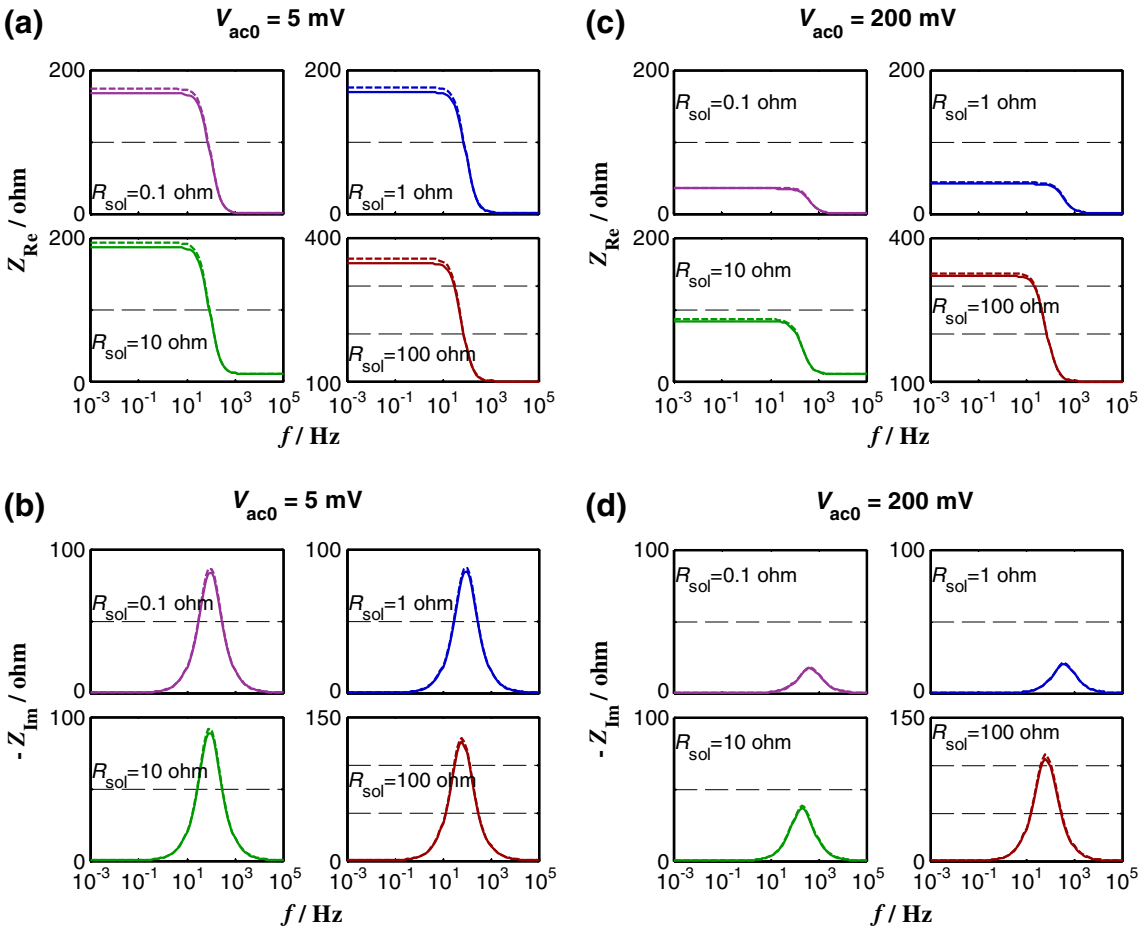

Fig. 6 Bode plots of real and imaginary components of the simulated impedance values and the KK transformed data, for various solution resistance values and two V_{ac0} values for the data in Fig. 5. *Dotted lines* are the original data and *solid lines* are the transformed data. In most cases, they completely overlap and are not distinguishable. Note that the scales are different for the plots with R_{sol}=100Ω

Reaction with adsorbed intermediate

Impedance spectra

Figure 7 shows the complex plane plots of impedance for V_{ac0}=10 mV, for various solution resistance values. Note that the solution resistance R_{sol} is subtracted from the real part of the impedance (Z_{Re}) to enable clear comparison. Two capacitance loops are observed for all the combinations of R_{sol} and V_{ac0}. It is known that for a reaction with a single adsorbed intermediate species, the Faradaic process will lead to an arc at low frequencies, while the double layer capacitance would lead to a capacitive arc at high frequencies [34, 35]. Since the value of the exponent b_1 is greater than b_2, two capacitive loops are seen. The results were qualitatively similar for all of V_{ac0} values employed.

The same data is presented in Fig. 8 as complex plane plots of the impedance spectra for a given value of R_{sol} and the two extreme values of V_{ac0}. This allows for a direct evaluation of the effect of changing V_{ac0} at a given R_{sol}. In Fig. 8a and b, the low-frequency impedance values for V_{ac0}= 200 mV are smaller than those for V_{ac0}=5 mV. It is shown in Fig. 8c that when the R_{sol} increases to 10Ω, the low-frequency impedance of the spectrum corresponding to V_{ac0}= 200 mV increases and moves towards that of V_{ac0}=5 mV. Thus, when R_{sol} is 10Ω, the spectra for all the V_{ac0} values would appear to be close to each other although they are not exactly identical. In particular, if the data were to be acquired experimentally the presence of noise would make it difficult to distinguish the spectra acquired at different V_{ac0} values. On the other hand, it must be noted that the impedance at the mid frequency also increases for V_{ac0}=200 mV when R_{sol} is changed from 1 to 10Ω (Fig. 8c vs Fig. 8b). Figure 8d shows that when the solution resistance is 100Ω, both the low and the medium frequency impedance values for V_{ac0}=200 mV are larger than those for V_{ac0}=5 mV. In summary, at low R_{sol} values, larger V_{ac0} result in smaller impedance values, at low frequencies. At large R_{sol} values, larger V_{ac0} actually result in higher impedance values, at mid and low frequencies. While the trends are clear and systematic, in the absence of analytical solution to the Eqs. 9 and 13, a simple physical picture of the processes explaining these trends does not seem to emerge.

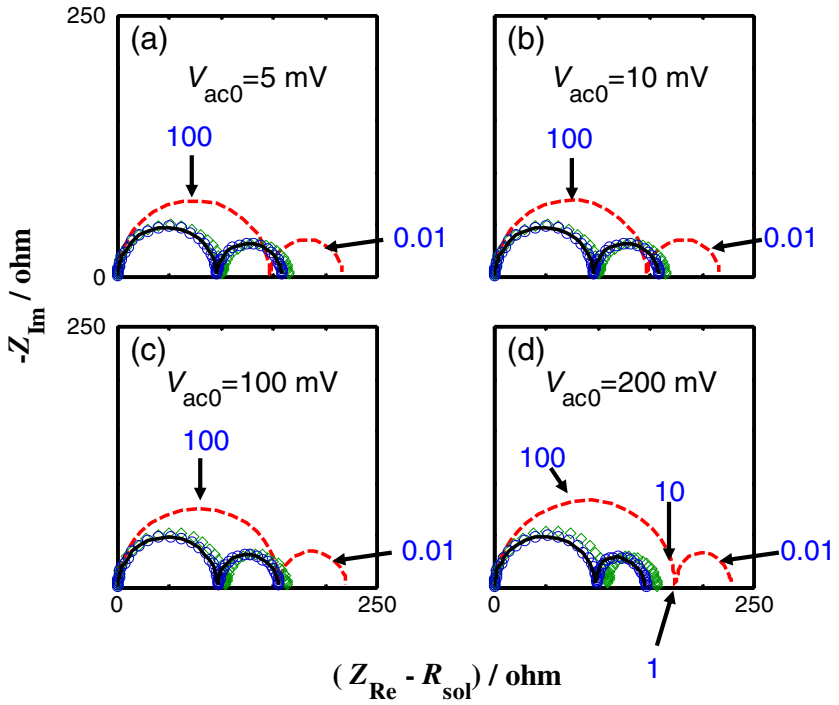

Fig. 7 Complex plane plots of impedance spectra for various V_{ac0} values for the reaction with adsorbed intermediate, given in Eq. 7. Note that in the abscissa, the solution resistance R_{sol} is subtracted from the real component of the impedance Z_{Re}. In each panel, R_{sol}: *solid line* 0.1Ω, *open circles* 1Ω, *open diamonds* 10Ω, *dashed line* 100Ω. For the most part, the impedance values for R_{sol}=0.1, 1 and 10Ω completely overlap. The parameter values are $k_{10}=10^{-11}$ mol s^{-1}, b_1=15 V^{-1}, $k_{20}=10^{-9}$ mol s^{-1}, b_2=5 V^{-1}, $\tau=10^{-7}$ mol, V_{dc}= 0.4 V, $C_{dl}=10^{-5}$ F. A few frequencies, in Hz, are marked in the figures

Kramers Kronig transforms

The impedance spectra in Fig. 8 are subjected to KKT and the results are presented in Fig. 9. The spectra were practically identical for V_{ac0}=5 and 10 mV for all the solution resistance values. Hence, only the cases of V_{ac0}= 10, 100 and 200 mV are presented in Fig. 9. Note that the dotted lines are the original values and the continuous lines are the transformed data. For V_{ac0}=10 mV, the original data and the transformed data match very well for most cases. Figure 9a shows that the real component values (Z_{Re}), at low frequencies, exhibit slight deviations and that the deviations are independent of R_{sol} values. A comparison of Fig. 9a and c shows that, for V_{ac0}= 100 mV, the match for the real component (Z_{Re}) is actually slightly better than that seen for V_{ac0}=10 mV. On the other hand, the imaginary

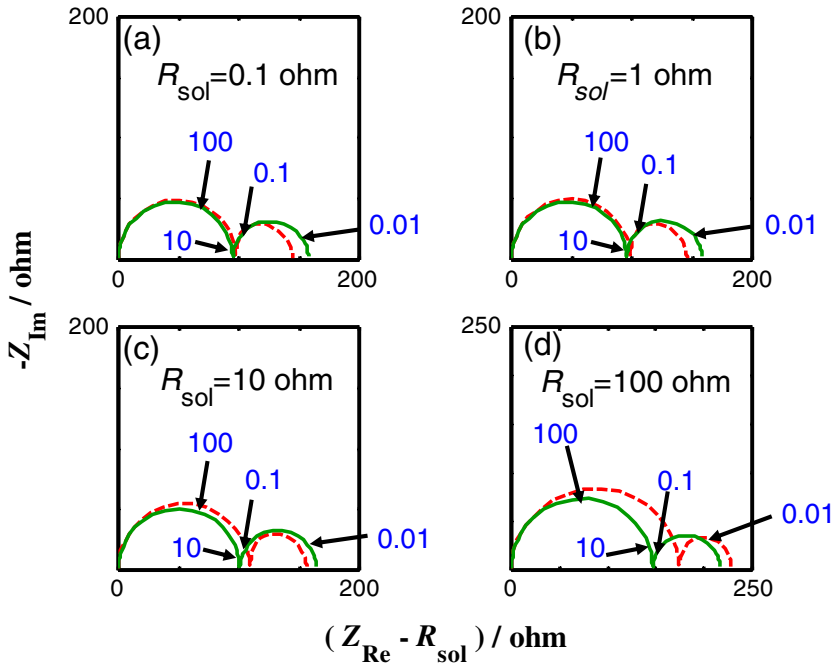

Fig. 8 Complex plane plots of impedance spectra for various R_{sol} values for the reaction with adsorbed intermediate, given in Eq. 7. Note that in the abscissa the solution resistance R_{sol} is subtracted from the real component of the impedance Z_{Re}. Note that the scales are different for R_{sol} of 100Ω case compared to other three cases. In each panel, V_{ac0}: *solid line* 5 mV, *dashed line* 200 mV. All parameters are the same as in Fig. 7. A few frequencies, in Hz, are marked in the figures

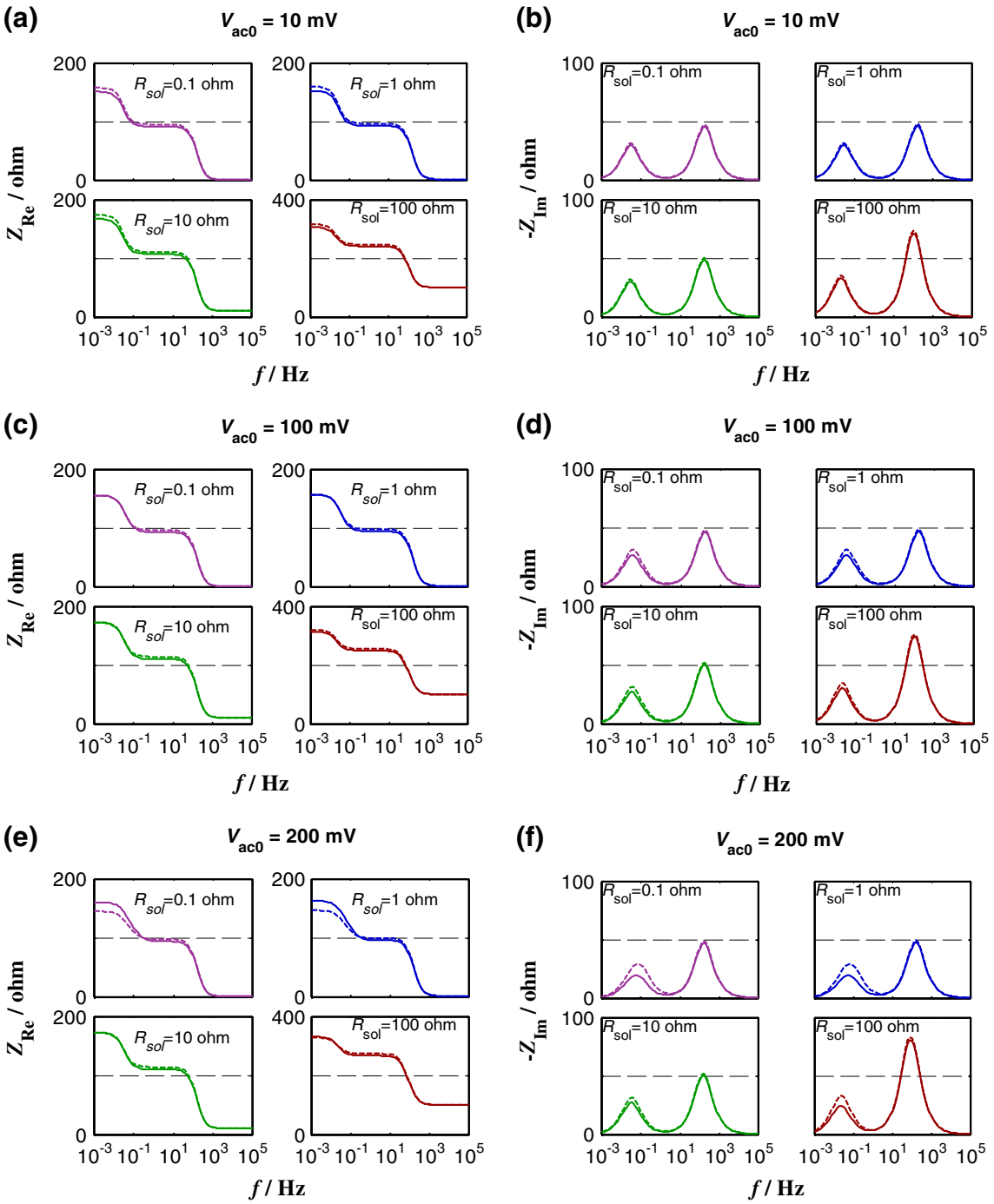

Fig. 9 Bode plots of real and imaginary components of the simulated impedance values and the KK transformed data, for various solution resistance values and V_{ac0} values for the data in Fig. 8. *Dotted lines* are the original data and *solid lines* are the transformed data. Note that the scales are different for the real component when R_{sol}=100Ω

component values ($-Z_{Im}$) near the peak at low frequencies in Fig. 9d show some deviations. However, the deviations are not particularly large, and in case of experimental data which contains some noise, these deviations may not be obvious. Finally, Fig. 9e and f shows that for the case of V_{ac0}=200 mV, for all values of R_{sol}, there are clear deviations between the transformed data and the original data, in both Z_{Re} and Z_{Im}. In fact it is more in the case when R_{sol}=0.1Ω compared to the case when R_{sol}=1Ω. This indicates that KKT identifies the nonlinear effect due to the large amplitude perturbation, but that it is not necessarily more sensitive if solution resistance is more. If KKT is sensitive to solution resistance effects, the deviations must be more when R_{sol}=100Ω and relatively less when R_{sol}=

0.1 Ω. Thus, KKT identifies the nonlinearities in this example, but its sensitivity is not enhanced by the solution resistance effects.

Reaction with two adsorbed intermediates

Current–potential relationship

Figure 10 shows the simulated current–potential diagram, calculated from Eq. 20 after setting the ac terms to zero. Note that the dc current (i_{2bdc}) shows a maximum and that the location of the peak depends on the R_{sol}. The surface coverage values of the adsorbed intermediates normally increase with the potential. The last step in Eq. 17 needs a vacant site. At high dc potentials (V_{dc}), the vacant sites will be less and hence beyond a certain potential, the dc current begins to decrease with the potential. The catalytic mechanism has been employed to explain the observed current–potential and EIS results for some metal corrosion phenomena [24, 25, 36–38]. Other physicochemical processes such as passivation by oxide growth or adsorption of inhibiting species can also result in a negative slope in the current–potential curve [39–44]. The electro oxidation of methanol on Pt electrode was studied in order to understand some of the processes in a direct methanol fuel cell [43]. At potentials above 650 mV vs hydrogen electrode, the impedance values occurred in the second quadrant of the complex plane plots and the blocking of adsorption sites by the chemisorbed hydoxy species was advanced as the cause of this behavior. The time dependent impedance spectra of methanol oxidation on Pt were measured and the negative impedance values observed were associated with the current oscillations [44]. Regardless of the origin, the presence of this negative slope leads to interesting impedance patterns with impedance values falling in the second and third quadrant of the usual complex plane plots of $-Z_{Im}$ vs Z_{Re}. Based on the values in Fig. 10, overpotential of 0.7 V was chosen and the impedance response at this potential is simulated.

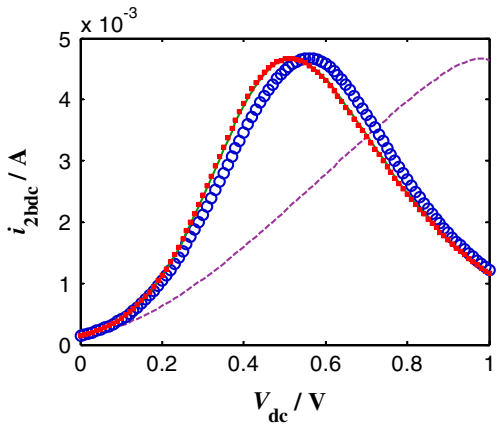

Fig. 10 The dc current vs applied dc potential for various solution resistance values, a reaction with negative resistance, given in Eq. 17. R_{sol}: *filled squares* 0.1 Ω, *solid line* 1 Ω, *open circles* 10 Ω, *dashed line* 100 Ω. The parameter values are $k_{10}=4\times10^{-7}$ mol s^{-1}, $b_1=0$ V^{-1}, $k_{-10}=8\times10^{-6}$ mol s^{-1}, $b_{-1}=-8$ V^{-1}, $k_{20}=10^{-9}$ mol s^{-1}, $b_2=2$ V^{-1}, $k_{-20}=3\times10^{-5}$ mol s^{-1}, $b_{-2}=-2$ V^{-1}, $k_{30}=2\times10^{-12}$ mol s^{-1}, $b_3=7$ V^{-1}, $k_{40}=5\times10^{-4}$ mol s^{-1}, $b_4=0$ V^{-1}, $\tau=9\times10^{-8}$ mol, $V_{dc}=0.7$ V, $C_{dl}=5$ 10^{-5} F

Impedance spectra

Figure 11 shows the complex plane plots for this mechanism at $R_{sol}=0.1\,\Omega$ and various V_{ac0} values. The inset shows the inner loop corresponding to $V_{ac0}=5$ mV. The mid frequency loop shows an inductive behavior while the low frequency loops shows negative resistance. Impedance spectra with very similar pattern have been reported in literature, as summarized below. The anodic dissolution of iron–chromium alloys in acidic sulfate media was investigated at various pH values and potentials [24, 25]. Complex plane plots of the measured impedance showed negative resistance values in the passivation region although none of the patterns were similar to the one presented in Fig. 11a. A fairly complex set of reactions involving the simultaneous oxidative dissolution of iron and chromium was proposed. The dissolution of iron in sulfate media at various pH values was studied [36]. At pH 5, at potential anodic of the onset of passivation, the impedance spectrum was similar to the one depicted in Fig. 11a. Although the measured pattern did not show negative resistance values, simulated impedance values based on a model which included a catalytic reaction predicted that negative resistance values would be observed. The model predicted the shapes of the impedance pattern at various pH values and potentials successfully. The transpassive dissolution of Ni in acidic sulfate media was examined using impedance spectroscopy [38]. Here also the impedance pattern, acquired at potentials anodic of the onset of passivation, portrayed a shape as shown in Fig. 11a.

The anodic oxidation of Ni, Sn, Cu and Sb in concentrated solutions was investigated [39]. At the initial stages, the dc current increased with the dc potential, but the formation of a passivating film caused a decrease in the current with an increase in the potential. A further increase in the potential resulted in transpassive dissolution. For all the systems analyzed, the impedance values measured in the transpassive regime exhibited negative resistance values in some frequencies, although the patterns were not similar to the one displayed in Fig. 11a. A metal–film–electrolyte model with a linear thickness–overvoltage relationship for the film and a reaction mechanism including a catalytic step was proposed. The anodic dissolution of Nb in acidic fluoride solutions and in warm alkali solution, as well as the dissolution of Mo in concentrated phosphoric acid was studied [40]. A saturated calomel electrode (SCE) was used as the reference electrode.

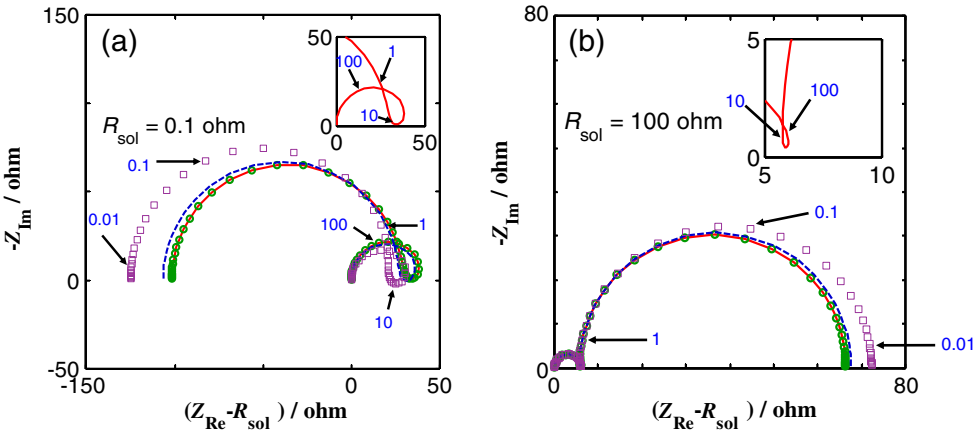

Fig. 11 Complex plane plots of impedance spectra for various R_{sol} values for the reaction with adsorbed intermediate, given in Eq. 17. Note that in the abscissa the solution resistance R_{sol} is subtracted from the real component of the impedance Z_{Re}. V_{ac0}: *solid line* 5 mV, *open circles* 10 mV, *dashed line* 100 mV, *open square* 200 mV. *Inset*: plot in the mid frequency, expanded for clarity. All parameters are the same as in Fig. 10. A few frequencies, in Hz, are marked in the figures

The oxide growth and the onset of passivation resulted in a negative current–potential plot. For Nb in 5 M NaOH at 60 C, at −0.875 V vs SCE in the passivation regime, the impedance plots were similar to Fig. 11a. The impedance of Mb in 14.8 M phosphoric acid, at 1.21 V vs SCE also exhibited the same shape. A metal–film–electrolyte model, with oxygen ion vacancy transport model for the film was employed to explain the results. The electro-oxidation of glucose on Ni–Cu alloy modified glassy carbon electrode was analyzed [41]. Both Ni and glucose were simultaneously oxidized and the current–potential curve showed a clear peak. At post peak potentials, the impedance diagrams showed negative resistance values. A kinetic model was proposed and the passivation of the electrode by one of the intermediate species of glucose oxidation was presumed to be the cause of the observed negative resistance values. The transpassive dissolution of Nb in acidic fluoride medium at various pH values was examined using EIS [42]. After the onset of passivation, at a potential of 0.1 V vs SCE, the impedance spectrum was qualitatively the same as that in Fig. 11a. The system was modeled using an equivalent electrical circuit model representing metal–film–electrolyte. The impedance of the film was derived from surface charge approach. The inductive loop at the mid frequencies was attributed to the elements associated to the negative surface charge at the oxide–electrolyte interface. Thus it is clear that negative resistances in general and the pattern shown in Fig. 11a in particular are not uncommon in EIS data of anodic dissolution of metal.

Figure 11a also shows that the nonlinear effects manifest only when $V_{ac0}\geq 100$ mV, since the spectra for $V_{ac0}=100$ mV is only slightly different from the spectra for $V_{ac0}=10$ mV. The spectra were qualitatively similar for $R_{sol}=1$ and 10Ω (Fig. S3). Figure 11b shows the results for $R_{sol}=100\Omega$ and it is qualitatively different from the spectra at Fig. 11a. Since the slope of the i_{2bdc} vs V_{dc} is positive for this case at $V_{dc}=0.7$ V, it is not surprising that the negative resistance is not observed in this case. Interestingly, in this example, for all R_{sol} values, the magnitude of low-frequency impedance (after accounting for R_{sol} values) was always larger for larger V_{ac0}.

Kramers Kronig transforms

The impedance values, along with the transformed values are presented for $V_{ac0}=5$ mV and various R_{sol} values in Fig. 12. The values, especially at low frequencies, are clearly different and appear more like mirror images, except for $R_{sol}=100\Omega$. The dissolution of Cu in acidic sulfate medium was studied near states close to instability [32, 45]. The system, exhibiting negative resistance, was analyzed from the perspective of non-minimum phase (nmp) systems. The minimum phase systems are those whose phase values are limited to $-\pi/2$ to $\pi/2$. It was shown for nmp systems, when the data are acquired under quasi potentiostatic control, KKT performed under admittance form is successful while that performed under impedance form fails. Electrical circuits with negative resistances and capacitances were used to simulate the impedance spectra with data in the second quadrant of the complex plane plots [33]. The expression for impedance was written as the ratio of two polynomials and the zeros and poles representation was used. The zero/pole representation has the advantage that it is unique while in the electrical circuit representation, more than one circuit can yield the same impedance spectra in the whole frequency range and hence it is not unique. When the KKT was performed on the impedance representation on systems unstable under quasi galvanostatic mode, then the low-frequency part of the spectrum was found to be non-compliant. But the KKT performed on the admittance representation of those systems was successful. In general, for systems which are stable only under quasi-potentiostatic control, the data will transform correctly under KKT only if the admittance form is used (assuming that the linearity, causality and stability criteria are satisfied) [3, 46].

The KK transforms were performed on the admittance form of the data and results, grouped by R_{sol} are presented in

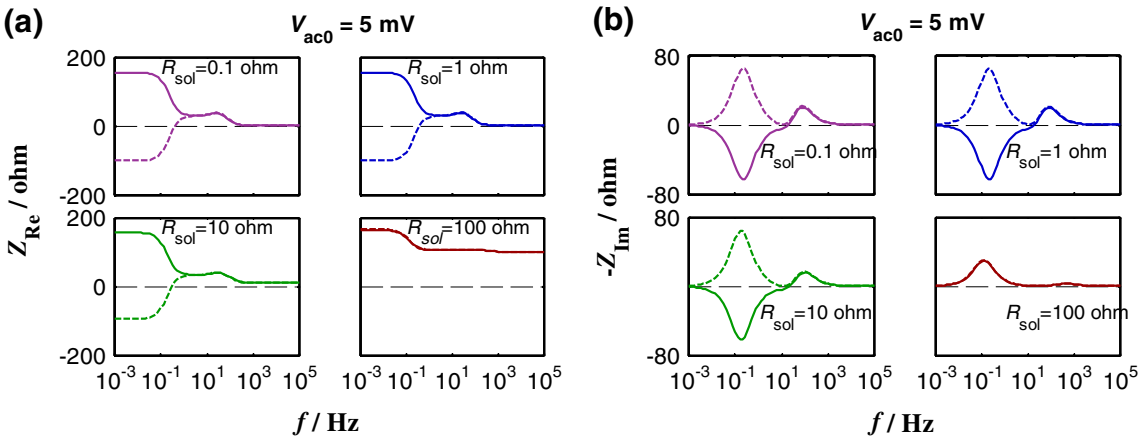

Fig. 12 Bode plots of real and imaginary components of the simulated impedance values and the KK transformed data, for various solution resistance values and V_{ac0} values for the data in Fig. 11. *Dotted lines* are the original data and *solid lines* are the transformed data. Note that both completely overlap for Z_{Re} and $-Z_{Im}$ for R_{sol}=100Ω

Fig. 13. For R_{sol}=0.1Ω, the real component of admittance (Y_{Re}) and the transformed values show a clear offset for all V_{ac0} values for most of the frequency range. The imaginary component (Y_{Im}) also shows a clear difference near the peak values as seen in Fig. 13b. The origin of this offset is not clear. The linearized versions of the equations were used to calculate the spectra and even they exhibited similar deviations (Fig. S4). One possibility is that the truncation

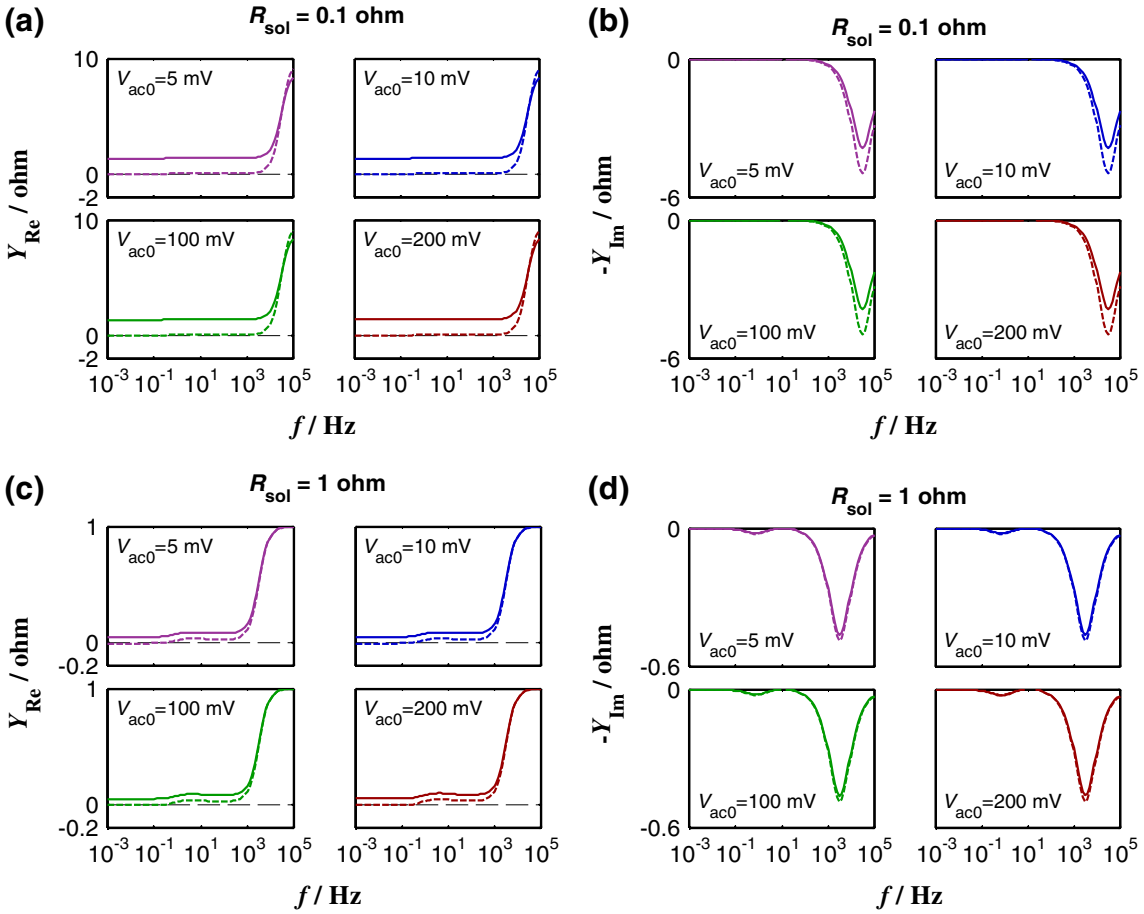

Fig. 13 Bode plots of real and imaginary components of the simulated admittance values and the KK transformed data, for various solution resistance values and V_{ac0} values for the data in Fig. 11. *Dotted lines* are the original data and *solid lines* are the transformed data. Note that both almost completely overlap for $-Y_{Im}$ values for R_{sol}=1Ω

of the frequency to a finite range in the transformations causes these deviations. Nevertheless, compared to the results in Fig. 12, it can be claimed that the trends in Fig. 13a and b show that the original and transformed values in admittance form are at least qualitatively similar. Figure 13c and d shows that at $R_{sol}=1\Omega$, the match between the original and transformed values is actually better. It is also worth noting that, for a given R_{sol}, the difference between the original and transformed values is not dependent on the V_{ac0} values. The same trend was seen for $R_{sol}=10\Omega$ (Fig. S5). Thus, in this example, KKT does not identify the violation of linearity criteria, and an increase in R_{sol} values does not enhance its sensitivity to detect these violations.

Conclusions

Numerical simulations were employed to determine the impedance spectra of electrochemical reactions with and without adsorbed intermediates, with significant solution resistance, under large amplitude perturbations. The governing nonlinear equations were numerically solved. When the solution resistance is significant, the average of the potential across the interface drifts and a sufficient wait time needs to be employed for the system to stabilize before acquiring EIS data. If the solution resistance is comparable to the charge transfer resistance, the impedance spectra is altered to a significant extent. In some cases, KKT identifies nonlinearities arising from large amplitude perturbations, but the sensitivity is independent of the solution resistance values. In some cases with negligible solution resistances, KKT does not identify the violations of the linearity criterion. In those cases, the introduction of solution resistance does not enhance the sensitivity of KKT to detect nonlinear effects.

Acknowledgement The authors are grateful to Prof. D.D. Macdonald (macdonald@matse.psu.edu) for the Kramers Kronig transform software.

References

1. Orazem M, Tribollet B (2008) Electrochemical impedance spectroscopy. Wiley, New Jersey
2. Barsoukov E, Macdonald JR (2005) Impedance spectroscopy. Wiley, New Jersey
3. Macdonald DD (2006) Electrochim Acta 51:1376–1388
4. Macdonald JR (1990) Electrochim Acta 35:1483–1492
5. Bojinov M (1997) Electrochim Acta 42:3489–3489
6. Gregori J, Garcia-Jareno JJ, Gimenez-Romero D, Vicente F (2005) J Solid State Elctrochem 9:83–90
7. Gregory J, Gimenez-Romero, Garcia-Jareno JJ, Vicente F (2006) J Solid State Electrochem 19:920–928
8. Nagendra Prasad Y, Vinod Kumar V, Ramanathan S (2009) J Solid State Electrochem 13:1351–1359
9. Epelboin I, Joussellin M, Wiart R (1981) J Electroanal Chem 119:61–71
10. Urquidi-Macdonald M, Real S, Macdonald DD (1990) Electrochim Acta 35:1559–1566
11. Darowicki K (1995) Corros Sci 37:913–925
12. Wilson JR, Schwartz DT, Adler SB (2006) Electrochim Acta 51:1389–1402
13. Kadyk T, Hanke-Rauschenbach R, Sundmacher K (2009) J Electroanal Chem 630:19–27
14. Diard JP, Le Gorrec B, Montella C (1997) Electrochim Acta 42:1053–1072
15. Darowicki K (1995) Electrochim Acta 40:439–445
16. Darowicki K (1997) Electrochim Acta 42:1781–1788
17. Darowicki K (1997) Electrochim Acta 42:1073–1079
18. Harrington DA (1997) Can J Chem 75:1508–1517
19. Hirschorn B, Tribollet B, Orazem ME (2008) Isr J Chem 48:133–142
20. Hirschorn B, Orazem ME (2009) J Electrochem Soc 156:C345–C351
21. Noyel Victoria S, Ramanathan S (2011) Electrochim Acta 56:2606–2615
22. Franceschetti D, Macdonald JR (1977) J Electroanal Chem 82:271–301
23. Macdonald JR, Franceschetti DR (1979) J Electroanal Chem 99:283–298
24. Keddam M, Mattos OR, Takenouti H (1986) Electrochim Acta 31:1147–1158
25. Keddam M, Mattos OR, Takenouti H (1986) Electrochim Acta 31:1159–1165
26. Macdonald DD, Real S, Smedley SI, Urquidi-Macdonald M (1988) J Electrochem Soc 135:2410–2414
27. Lee WJ (2003) Mater Sci Eng A 348:217–226
28. Wong DKY, Coller BAW, Macfarlane DR (1993) Electrochim Acta 38:2121–2127
29. Macdonald DD (1990) Electrochim Acta 35:1509–1525
30. Macdonald DD, Urquidi-Macdonald M (1985) J Electrochem Soc 132:2316–2319
31. Urquidi-Macdonald M, Real S, Macdonald DD (1986) J Electrochem Soc 133:2018–2024
32. Sadkowski A, Dolata M, Diard JP (2004) J Electrochem Soc 151: E20–E31
33. Sadkowski A, Diard JP, Montella C (2009) J Electrochem Soc 156:F7–F13
34. Diard JP, Le Gorrec B, Montella C (1992) J Electroanal Chem 326:13–36
35. Maddala J, Krishnaraj S, Vinod Kumar V, Ramanathan S (2010) J Electroanal Chem 638:183–188
36. Keddam M, Mattos OR, Takenouti H (1981) J Electrochem Soc 128:257–266
37. Keddam M, Mattos OR, Takenouti H (1981) J Electrochem Soc 128:266–274
38. Keddam M, Takenouti H, Yu N (1985) J Electrochem Soc 132:2561–2566
39. Bojinov M (1996) J Electroanal Chem 405:15–22
40. Bojinov M, Cattarin S, Musiani M, Tribollet B (2003) Electrochim Acta 48:4107–4117
41. Danaee I, Jafarian M, Forouzandeh F, Gobal F, Mahjani MG (2008) J Phys Chem B 112:15933–15940
42. Cattarin S, Musiani M, Tribollet B (2002) J Electrochem Soc 149: B457–B464
43. Melnick RE, Palmore GTR (2001) J Phys Chem B 105:1012–1025
44. Melnick RE, Palmore GTR (2001) J Phys Chem B 105:9449–9457
45. Sadkowski A (2005) Solid State Ionics 176:1987–1996
46. Gabrielli C, Keddam M, Takenouti H (1993) Kramers Kronig Transformation in relation to the interface regulating device. In: Scully JR, Silverman DC, Kendig MW (eds) Electrochemical impedance: analysis and interpretation STP 1188. ASTM, Philadelphia, pp 140–153